Title

Propagation of Gaussian and Laguerre-Gaussian vortex beams through mouse brain tissue

Journal

Journal of Biophotonics, 10(12)

ISSN

1864-063X

Authors

Shi, Lingyan

Lindwasser, Lukas

Wang, Wubao

et al.

Publication Date

2017-12-01

DOI

10.1002/jbio.201700022

Peer reviewed

HHS Public Access

Author manuscript

J Biophotonics. Author manuscript; available in PMC 2018 December 01.

Published in final edited form as:

J Biophotonics. 2017 December ; 10(12): 1756–1760. doi:10.1002/jbio.201700022.

Propagation of Gaussian and Laguerre-Gaussian Vortex Beams through Mouse Brain Tissue

Lingyan Shi[1,2,3,*], **Lukas Lindwasser**[1], **Wubao Wang**[1], **Adrián Rodríguez-Contreras**[1,2], and **Robert Alfano**[1]

[1]Institute for Ultrafast Spectroscopy and Lasers, Department of Physics, The City College of the City University of New York, 160 Convent Avenue, New York, NY 10031, USA

[2]Department of Biology, The City College of the City University of New York, 160 Convent Avenue, New York, NY 10031, USA

[3]Department of Chemistry, Columbia University, New York, NY 10027, USA

Abstract

Light transmission of Gaussian (G) and Laguerre-Gaussian (LG) vortex beams in mouse brain tissue is investigated. Transmittance is measured with different orbital angular momentums (OAM) at various tissue thicknesses. In both ballistic and diffusive regions, transmittances of G and LG beams show no significant difference. The transition point from ballistic to diffusive region for the mouse brain tissue is determined at about 480 μm. The observed transmittances of the G and LG beams show independence on OAM modes, which may be attributed to poorly understood interference effects from brain tissue.

Keywords

Laguerre Gaussian beam; vortex; propagation; brain; ballistic light

1. Introduction

In brain research, imaging technique is always a major challenge for achieving better resolution and deeper imaging depth. Magnetic resonance imaging (MRI) has been widely applied in clinical and basic research for brain imaging, but its spatial resolution can only reach mm-scale. Optical imaging is still the only technique that can offer imaging resolution at micrometer or sub-micrometer scale. However, light experiences great scattering and absorption when it propagates through the brain tissue, due to the unique composition of the brain that contains twice the amount of lipids and less than half the amount of protein compared to muscle [1], which limits the penetration depth to several hundred micrometers.

The motivation behind the focus of the paper arises from light's salient properties that can be used for imaging: wavelength, polarization, coherence, and wavefronts. Some of these have

*Corresponding Author: Robert Alfano ralfano@ccny.cuny.edu.

been used in experimental and theoretical studies to image deeper into model of scattering media and tissues.

Various optical techniques and methods have been developed and employed to increase the imaging depth in tissues from these properties. Examples are: 1) multiphoton microscopy for fluorescence imaging because of its excellent penetration in scattering tissue; 2) gradient index (GRIN) lens together with multiphoton microscopy that extends the imaging depth to several millimeters in mouse brain [2, 3]; 3) the coherence is used for ballistic light in OCT; 4) using four optical windows in the near-infrared (NIR) region (650 – 2500 nm) that greatly reduce light scattering and absorption and achieve deeper brain imaging in which the excitation or emission wavelength falls within the third optical window (1600 – 1870 nm, named “Golden Window”) [4]; and 5) two-photon second singlet excitation technique for fluorescence agents [5] that greatly improves imaging depth in rat brain tissue where both the excitation and emission wavelengths fall within the optical window.

Regarding polarization, Alfano and co-worker [6] showed that circularly polarized light (CP) travels deeper than linearly polarized light (LP) for large particles ($a > \lambda$). CP scattering is highly forward and anisotropic. The transmitted light depolarization length for CP is larger than the corresponding length for LP light for large particle scattering [6].

In the optical process, lasers are commonly used as the sources to generate coherent lights. Among these, a fundamental (lowest) transverse mode of light is the Gaussian (G) beam, whose electric field amplitude is a solution to the paraxial Helmholtz equation and has a Gaussian intensity profile. A higher order mode solution of the paraxial wave equation is the Laguerre-Gaussian (LG) beam, the electric field amplitude of which is given by [7

$$E(r,\phi,z)=\frac{C_{\mathrm{lp}}^{\mathrm{LG}}}{w(z)}\left(\frac{r\sqrt{2}}{w(z)}\right)^{|l|}\exp\left(-\frac{r^2}{w^2(z)}\right)L_p^{|l|}\left(\frac{2r^2}{w^2(z)}\right)\times\exp\left(-\mathrm{ik}\frac{r^2}{2R(z)}\right)\exp\left(\mathrm{il}\phi\right)\exp\left[i(2p+|l|+1)\xi(z)\right] \quad (1)$$

where, r is the radial distance from the center axis of the beam, ϕ is the azimuth, z is the axial distance from the beam’s waist, C_{lp}^{LG} is an appropriate normalization constant, $w(z)$ is the beam width as a function of z, l is the azimuthal index (also known as the topological charge), L_p^l are the generalized Laguerre polynomials, i is the imaginary unit, $k = 2\pi/\lambda$ is the wave number for a wavelength λ, $R(z)$ is the radius of curvature of the beam’s wavefronts at z, p is the radial index ($p \geq 0$), and $\xi(z)$ is the Gouy phase shift at z. When $p = 0$ and $l = 0$, Eq. (1) gives a G beam, characterized by a planar wavefront; for $l \neq 0$ (and $p = 0$), Eq. (1) gives a LG vortex beam that having a helical wavefront and an orbital angular momentum (OAM). The LG beam is characterized by the spiral (vortex) phase term $\exp(il\phi)$, which is dependent on the topological charge l and has a phase singularity at the center of the helical wavefront.

The LG and G beams are most used in laser-material interaction optics and beam propagation in multiphoton application and imaging, but much less used to probe light-tissue interactions. The application of G beams for imaging rat brain microvessels using two photon microscopy has been recently examined [8]. Applications of LG beam in laser-matter interaction optics have been investigated extensively during the past decade [9–23]. Experiments using vortex beam in phase contrast imaging (so-called spiral phase contrast) showed the complete suppression of the background and a strong and isotropic edge enhancement in objects [9, 10]; the edge enhancement can also be anisotropic with preferred direction and degree by controlling the phase of the vortex beam [11–12], as discussed and reviewed in detail by Maurer et al. [13]. Schwartz and Dogariu used vortex beam study the enhanced backscattering cone in volume scattering media [14–16]. Their theoretical prediction and experimental measurement both demonstrated a linear relationship between the backscattering enhancement and the topological charge of the vortex beam. In addition, scattering properties of the medium such as the transverse scattering length and diffusion coefficient can be obtained by modifying the enhanced backscattering cone using a singular (vortex) beam. Vortex beam microscopy avoids the diffraction limit in spatial resolution and experiments demonstrated an imaging sensitivity at 20 nm and a working distance of 1 mm [17]. Similarly, using a vortex beam created by the reflected field of sub λ-structure, Eberler and colleagues [18] obtained high precision properties of the object that was limited by classical microscopy. Recently, Schmiegelow and colleagues [19] excited an atomic transition with LG vortex beams and observed the transfer of LG beam OAM to a bound electron. Their study showed that the OAM could influence the motion state of bound electrons, and change the selection rules of optical excitation. Therefore, OAM can be utilized to control light-matter interaction, nevertheless, it is still controversial since such OAM light-matter interactions were not found in some other theoretical and experimental studies [20–23].

There are still few studies using the LG beam to probe light-tissue interactions, especially in brain imaging. Biological tissues are more likely “phase objects” rather than “amplitude objects” [13]. Applying vortex beams with different topological charges in brain imaging may affect light-tissue interaction and improve the backscattering effect. It is thus tempting to hypothesize that LG beams would penetrate deeper in turbid scattering media compared to G beams, and since brain tissue is a highly-scattering medium, applying LG beams for brain imaging may realize higher penetration depths compared to G beams.

In this study, light transmission of LG vortex beams with different OAMs through mouse brain tissues was measured and compared with a G beam. The motivation to use LG for deeper imaging arises from our past work using NIR wavelengths and CP vs LP polarized light [4, 6].

2. Material and Methods

2.1. Experimental Setup

Figure 1 shows the schematic of the experimental setup. A He-Ne laser (5 mW, excitation wavelength 633 nm) was used as the light source. The laser beam was focused onto a single-mode optical fiber (SMOF). The output beam from the optical fiber passed through a lens,

reached the first beam splitter (BS1), and illuminated the spatial light modulator (SLM, HoloEye LC-R 720) that was working in the reflection mode. The LG beam was generated by the SLM. Different OAMs of LG beam could be obtained by different forked diffraction patterns of the SLM. The generated LG beam was then split into a sample beam and a reference beam by the second beam splitter (BS2). The sample beam passed through a mouse brain tissue sample. The reference beam was used to monitor and take account of the change of incident light in calculating the transmittance. Both the sample beam and reference beam were recorded simultaneously by a CCD camera (16-bit, FLI Finger Lakes Instrumentation, Lima, NY). The topological charge l values were chosen to be 0, and 1–8 for the G and LG beams, respectively. The beam waist increased with increasing l, with a beam waist bounded above by 400μm (The size of the aperture (A) in Figure 1). However, the difference between the position of the image between lenses (L4) and (L5) for the beam of charge 0 and 8 was negligible. Thus, the different beam waists did not significantly affect the results discussed below.

2.2. Brain Tissue Preparation

The brain tissue samples were prepared following the procedures approved by the Institutional Animal Care and Use Committee (IACUC) of the City College of New York. An adult mouse was anesthetized by injection of a mixture of ketamine and xylazine (41.7 and 2.5 mg/kg, body weight, respectively). After the mouse was completely anesthetized, it was perfused intracardially with 4% formaldehyde in 0.1 M phosphate buffer (PB) at cardiac output rate using a syringe pump [4]. The brain was dissected and post-fixed overnight, and subsequently immersed in 30% sucrose in 0.1 M PB for up to 48 hours before slicing. The brain tissue was sliced by using a freezing stage microtome (American Optical, Buffalo, NY) at 14 different thicknesses (60, 120, 180, 240, 300, 360, 480, 540, 600, 720, 1320, 1860, and 2340 μm, respectively). The accuracy in tissue slice thickness was ±2 μm.

2.3. Data Collection

The light transmittance was calculated as the ratio of the sample beam intensity to the reference beam intensity. The same image areas, hence the same numbers of CCD pixels, were chosen for both G and LG beams. The calculated transmittance was analyzed with respect to different tissue thickness and topological charge (l) of LG beams.

3. Results and Discussion

Figure 2 shows the transmittance (T) of LG beams as a function of mouse brain tissue thickness z at different topological charges l. The dashed line without markers is the curve fitting result by using equation $T = e^{-\mu z} + Ce^{-\kappa z}$ [24], where $\mu = 1.04 \times 10^{-2}$ μm^{-1}, $C = 1.12 \times 10^{-2}\kappa = 6.37 \times 10^{-4}$ μm^{-1}, and z is tissue thickness. The first term of the fitting equation corresponds to the ballistic component and the second term the diffusive component [4].

It can be seen from Figure 2 that the transition from ballistic region to diffusive region occurs at about 480 μm, where the decay slopes change significantly [4, 24, 25]. Within the ballistic region, non-scattered light dominates, and the decay of T falls rapidly with thickness following Beer's law. The attenuation length could be extracted from the fitting to

be $l_{\text{ballistic}}$ = 0.22 mm, which is close to the value 0.194 mm measured by Shi et al. [4]. In the diffusive region where multiple scattering is dominant, decay rates of T slow down. The attenuation length was fitted to be $l_{\text{diffusive}}$ = 0.22 mm. In both regions, the G and LG beams show no obvious differences in transmittance, and both beams are independent of the topological charge l when propagating in brain tissue.

Figure 3 shows the transmittance T as a function of topological charge l of LG beams for mouse brain tissues at thicknesses of 60, 480, and 2340 μm, respectively. It can be seen that T of G beam (l = 0) in thick brain tissue (2340 μm) is slightly higher than that of LG beams ($l \geq 1$) but the difference is not significant; the T of LG beams shows the independence on the topological charge l, although the T obviously reduces with tissue thickness z.

Our experimental results indicate that the G and LG beams showed no significant difference in transmittance through mouse brain tissue at 60 to 2340 μm thick in both the ballistic and diffusive regions, i.e. the transmittance of LG beams in mouse brain tissue is independent of the topological charge l. The transition from ballistic to diffusive region was found at thickness 480 μm. Another salient feature is the slow oscillatory behavior in the ballistic region shown in Figure 2, which occurs at a distance of about 120 μm. This behavior may arise from the interference between the ballistic, snake, and diffusive parts, where the interference is characterized by the third term in the following equation [26]:

$$I = I_B + I_D + 2(I_B I_D)^{1/2}\cos\varphi \quad (2)$$

where φ=kz, I_B and I_D are ballistic and diffusive intensity, respectively, for any pathway that photons travel in the brain tissue. The independence of transmittance on the topological charge l suggests that photons propagate through neural tissue without depending on chirality of the LG beam.

The brain tissue is made up of numerous neurons and cells. Both neurons and cells according Zamorano and Torres Silva [27] can be taken as chiral media being considered as a chiral bioplasma. There is always great interest in probing the interaction of vortex light with chiral molecules. However, theoretical studies obtained controversial results. Our experiments does not support chiral concept and showed no significant difference in LG and G beams transmitting through brain tissue, suggesting that LG beam, carrying an OAM, does not interact with spatial resonance in the chiral brain tissue. It is consistent with the theoretical study [21] and experimental results that did not find any influence of vortex light interaction on the circular dichroism of chiral matter [22, 23].

Deep brain imaging has always been an important area for neuroscience. In this study, transmission of LG and G beams through brain tissue were collected by a CMOS camera. Future studies of LG vortex beams for brain imaging may use phase contrast microscopy to better understand vortex light–brain tissue interaction, or use multiphoton microscopy, which offers a nonlinear optical process, for deep brain imaging with better resolution. In-depth studies are needed in the future to better understand the scattering properties of LG

and G beams in brain and other tissues. There should be special pathways in brain to propagate information.

4. Conclusion

Our study showed that transmissions of LG and G beams in mouse brain tissue displayed similar dependence on tissue thickness, and were independent of topological charge for brain tissue thickness ranging from 60 to 2340 μm. Future studies are necessary for further validation and better understanding of the underlying physics. To the best of our knowledge, this is the first study that measured transmission of LG vortex and G beams through mouse brain tissue. We hope this study would inspire more experimental as well as theoretical studies on LG vortex beams propagating in brain tissue, for developing new techniques and methods in deep brain imaging.

Acknowledgments

The research was supported in parts by U. S. Army Research Office (ARO) through grant #W911NF-13-1-0151, and industrial companies of NxGEN and Corning. NIH grants 5SC1HD068129 (ARC), and 2G12RR003060-26A1 from the National Center for Research Resources (ARC). We thank Dr. Luyao Lu for her help in preparing brain tissue samples, and Dr. Dan Nolan and Dr. Solyman Ashrafi for their helpful discussions.

References

1. McIlwain, H., Bachelard, HS. Biochemistry and the Central Nervous System. Churchill Livingstone; Edinburgh; New York: 1985.
2. Murray T, Levene MJ. J. Biomed. Opt. 2012; 17:021106. [PubMed: 22463024]
3. Levene MJ, Dombeck DA, Kasische KA, Molloy RP, Webb WW. J. Neurophysiol. 2004; 91:1908–1912. [PubMed: 14668300]
4. Shi L, Sordillo LA, Rodriquez-Contreras A, Alfano RR. J. Biophotonics. 2016; 9:38–43. [PubMed: 26556561]
5. Shi L, Rodriquez-Contreras A, Budansky Y, Pu Y, Nguyen TA, Alfano RR. J. Biomed. Opt. 2014; 19:066009. [PubMed: 24967915]
6. Ni X, Alfano RR. Opt. Lett. 2004; 29:2773–2775. [PubMed: 15605501] Xu M, Alfano RR. Phys Rev. E. 2005; 72(12):065601.
7. Wang WB, Gozali R, Shi L, Lindwasser L, Alfano RR. Opt. Lett. 2016; 41:2069–2072. [7]. [PubMed: 27128076]
8. Shi L, Rodriquez-Contreras A, Alfano RR. J. Biomed. Opt. 2014; 19:126006. [PubMed: 25490048]
9. Fürhapter S, Jesacher A, Bernet S, Ritsch-Marte M. Opt. Express. 2005; 13:689–694. [PubMed: 19494929]
10. Crabtree K, Davis JA, Moreno I. Optical processing with vortex-producing lenses. Appl. Opt. 2004; 43:1360. [PubMed: 15008542]
11. Jesacher A, Fürhapter S, Bernet S, Ritsch-Marte M. Phys. Rev. Lett. 2005; 94:233902. [PubMed: 16090473]
12. Situ, Guohai, Warber, Michael, Pedrini, Giancarlo, Osten, Wolfgang. Phase contrast enhancement in microscopy using spiral phase filtering. Opt. Commun. 2010; 283:1273–1277.
13. Maurer C, Jesacher A, Bernet S, Ritsch-Marte M. Laser Photonics Rev. 2011; 5:81–101.
14. Schwartz C, Dogariu A. Opt. Commun. 2006; 263:135–140.
15. Scheartz C, Dogariu A. Opt. Lett. 2005; 30:1431–1433. [PubMed: 16007764]
16. Scheartz C, Dogariu A. Opt. Commun. 2006; 258:79–89.
17. Spektor B, Normatov A, Shamir J. Appl. Opt. 2008; 47:A78–A87. [PubMed: 18239703]
18. Eberler M, Quabis S, Dorn R, Leuchs G. Proc. SPIE. 2002; 4777:362–370.

19. Schmiegelow CT, Schulz J, Kaufmann H, Ruster T, Poschinger UG, Schmidt-Kaler F. Nat. Commun. 2016; 7:12998. [PubMed: 27694805]
20. Babiker M, Bennett CR, Andrews DL, D´avila Romero LC. Phys. Rev. Lett. 2002; 89:143601. [PubMed: 12366045]
21. Andrews DL, D´avila Romero LC, Babiker M. Opt. Commun. 2004; 237:133–139.
22. Araoka F, Verbiest T, Clays K, Persoons A. Phys. Rev. A. 2005; 71:055401.
23. Löffler W, Broer DJ, Woerdman JP. Phys. Rev. A. 2011; 83:065801.
24. Alfano, RR., Wang, WB., Wang, L., Gayen, S. Photonics, Volume IV: Biomedical Photonics, Spectroscopy, and Microscopy. Andrews, D., editor. Willey; 2015. p. 367-412.
25. Kempe M, Genack AZ, Rudolph W, Dorn P. J. Opt. Soc. Am. A. 1997; 14:216.
26. Born, M., Wolf, E. Interference and Diffraction of Light. Cambridge University Press; Cambridge: 1999. Principles of Optics: Electromagnetic Theory of Propagation.
27. Zamorano M, Torres Silva H. Phys. Med. Biol. 2006; 51:1661–1672. [PubMed: 16552096]

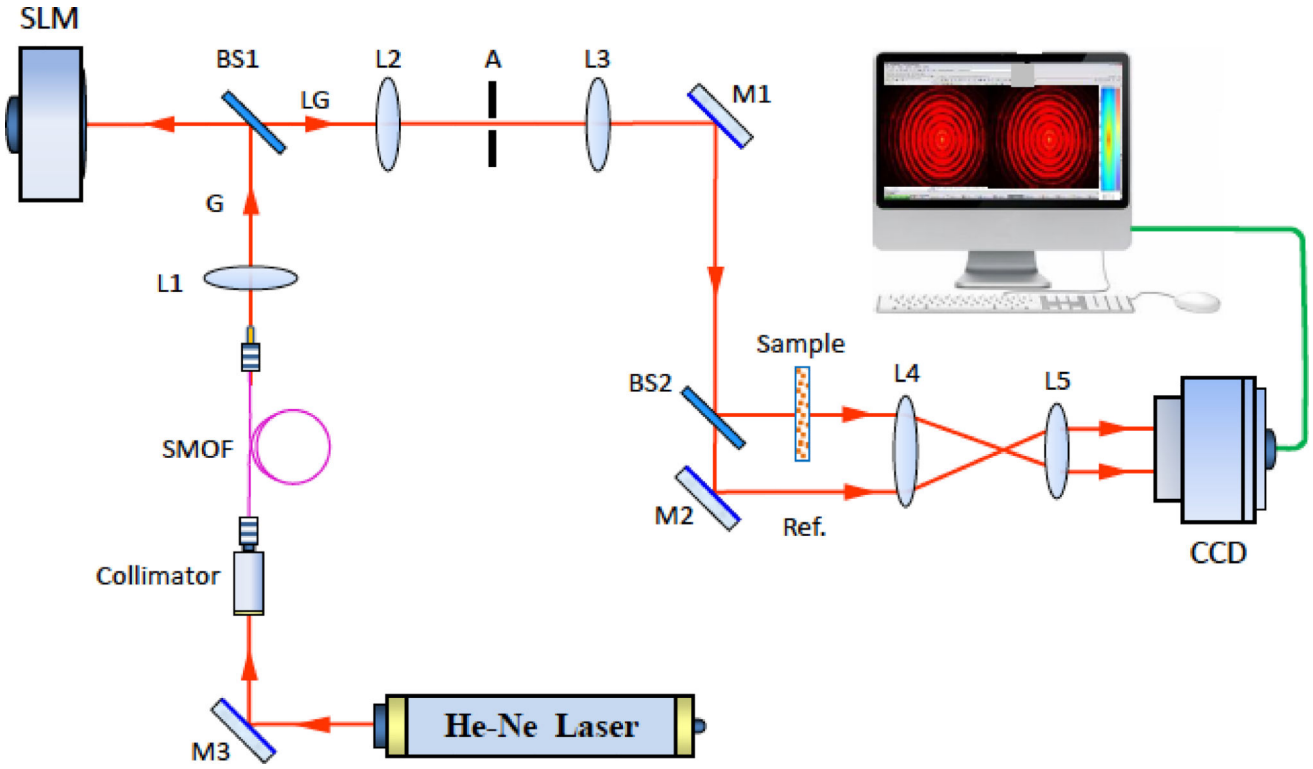

Figure 1.

Experimental setup. SMOF, single mode optical fiber; L, lenses; G, Gaussian beam; BS, beam splitter; SLM, spatial light modulator; LG, Laguerre-Gaussian beam; A, aperture; M, mirrors; CCD, charge coupled device camera.

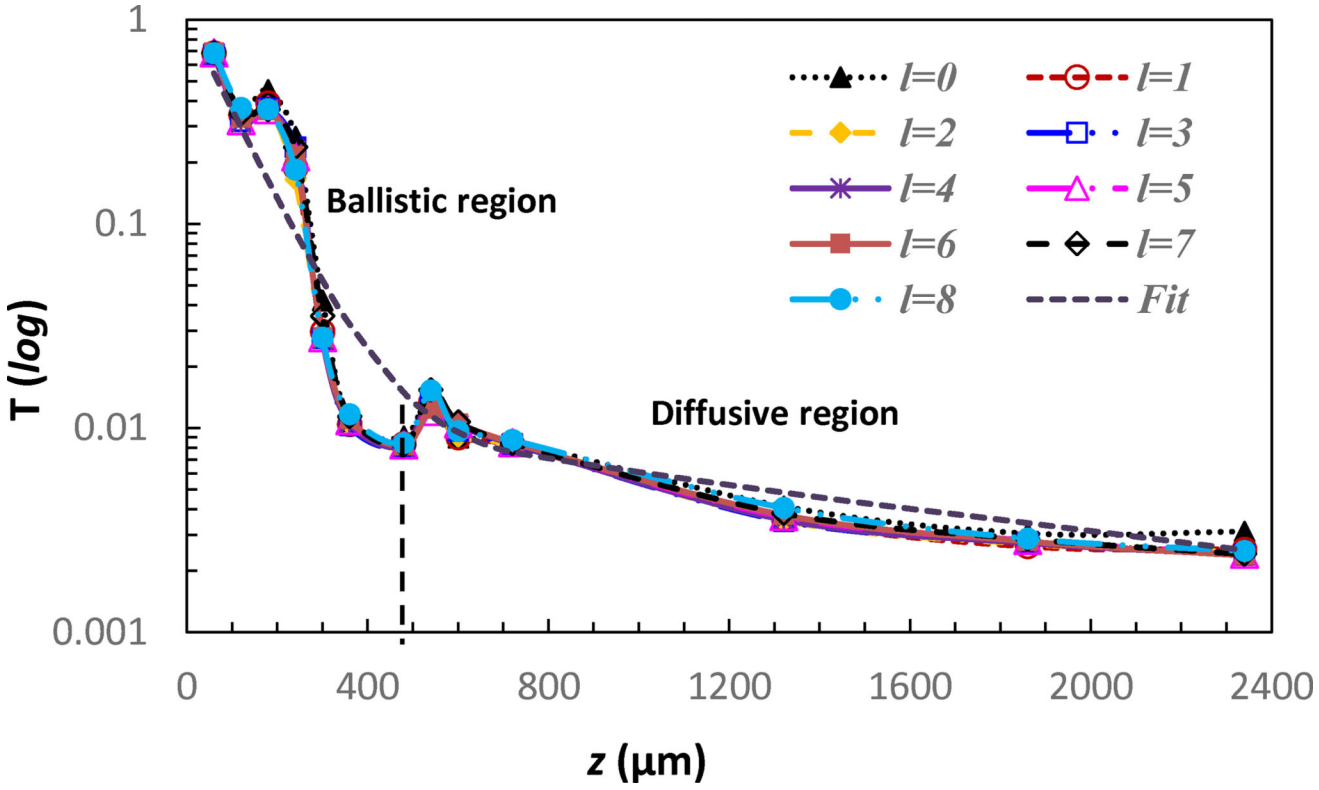

Figure 2.

Transmittance (T) as a function of tissue thickness (*z*) at different topological charge *l*. Dashed curve is the theoretical fitting by equation $T=e^{-\mu z}+Ce^{-\kappa z}$, where $\mu=0.010403\ \mu m^{-1}$, $C=0.0112$, and $\kappa=6.3693\times10^{-4}\ \mu m^{-1}$.

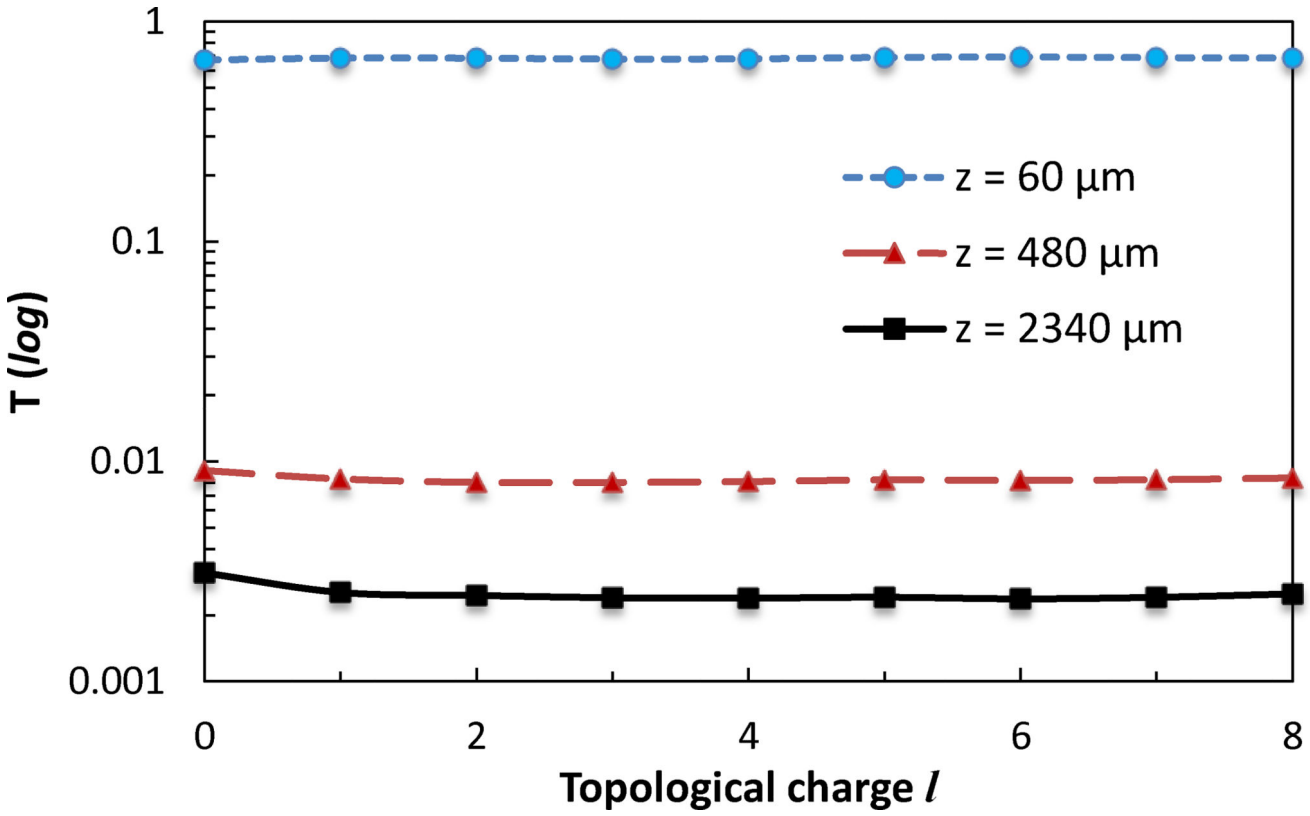

Figure 3.

Transmission as a function of topological charge *l* of LG beams with tissue thickness z = 60 µm, 480 µm, and 2340 µm respectively.